JOURNAL OF SPACECRAFT AND ROCKETS
Vol. 43, No. 6, November–December 2006

Generator Regime of Self-Balanced Electrodynamic Bare Tethers

J. Peláez* and M. Sanjurjo*
Technical University of Madrid, 28040 Madrid, Spain

DOI: 10.2514/1.20471

The generator regime of electrodynamic bare tethers working at inclined orbits is analyzed. Without damping or some kind of control, the attitude dynamics of these tethers is unstable. However, the instability disappears, or reduces drastically, when the tether is self-balanced, that is, when the Lorentz torque about the system center of mass vanishes. The aim of the paper is to describe in detail the main parameters involved in the dynamics of this type of tether and also their influence on the balance condition. In addition, a strategy will be proposed to keep the tether balanced, taking into account the whole trajectory followed by the system during the deorbiting process.

Nomenclature

$\hat{f}$	=	factor of ε, see Eq. (28)
f_g	=	growth factor
G	=	system center of mass
$Gxyz$	=	orbital frame
h	=	distance from the upper end, m
I_C	=	tether current at the cathodic end, A
I_e	=	tether current, A
$I_{\rm sc}$	=	short-circuit current, A
i	=	orbital inclination, rad
i_B	=	nondimensional maximum tether current
i_C	=	nondimensional version of I_C
i_e	=	nondimensional tether current
L	=	tether length, m
L_*	=	characteristic bare tether length, m
L_B	=	anodic segment length, m
ℓ_t	=	nondimensional tether length L/L_*
m	=	whole system mass, kg
$m_{\rm t}$	=	tether mass, kg
$m_1(m_2)$	=	lower (upper) end mass, kg
$\vec{\boldsymbol{u}}$	=	unit vector along the tether
$V_{\rm cc}$	=	potential drop in the cathodic contactor, V
W_d	=	power dissipated in the whole system, W
W_g	=	power generated in the interposed load, W
ε	=	nondimensional parameter defined in Eq. (6)
ε_0	=	factor of ε, see Eq. (28)
η_t	=	tether efficiency as deorbiter, see Eq. (35)
θ	=	in-plane angle, rad
Λ_t	=	tether mass, percentage
ξ	=	nondimensional distance from the upper end
ξ_B	=	nondimensional value of $L_{\rm B}$
σ	=	electrical conductivity, $\text{ohm}^{-1} \cdot \text{m}^{-1}$
ϕ	=	mass angle, rad
ϕ^*	=	critical value for a balanced tether, rad
φ	=	out-of-plane angle, rad
φ_e	=	nondimensional potential bias
Ω	=	nondimensional interposed load

Introduction

DEORBITING of satellites from low Earth orbits (LEOs) at the end of their operational life has been suggested as a feasible and attractive application of electrodynamic tethers, especially in the field of space debris mitigation. These devices are able to exert electrodynamic drag at heights where the aerodynamic drag is negligible (e.g., 2000 km). This production of drag is reliable, cheaper than other solutions and can be used to deorbit satellites at the end of their lifetime (and also other types of space debris). An electrodynamic tether does not use fuel to deorbit space debris; quite the opposite, it can recover a significant part of the orbital energy of the debris to be deorbited during the process, if this option is considered advisable. These significant advantages of electrodynamic tethers means that they are soon likely to play a decisive role in deorbiting.

There are two basic configurations for an electrodynamic tether: 1) the insulated tether, with current collection and emission only at end masses, and 2) the bare tether, with current collection along its anodic portion. Moreover, an electrodynamic tether has two basic operation regimes: the thruster mode and the generator (deboost) mode.

Apart from the polar band (orbital inclination $i \simeq 85$–90 deg) where the vertical tether is not appropriate, most satellites are present in the midinclination band ($i \simeq 40$–60 deg). However, when an electrodynamic tether operates in an inclined orbit, its attitude is affected by a dynamic instability due to the electrodynamic forces acting on the system. This skip rope type of instability has been detected previously and explained in [1–4] and it appears for any tether configuration and for any operation regime. It has also been studied previously (see [5–9]), and was detected in several dynamic simulations [10,11]. Because the averaged tether current is considered constant along the orbit and, in particular, independent of the actual tether position, the previously reported analyses can be applied to both tether configurations and both operation regimes.

The instability appears in the motion relative to the system center of mass G and depends on the Lorentz torque about G, which is proportional to a nondimensional parameter ε [see Eq. (6)]. This parameter gauges the Lorentz torque vs the torque produced by the gravity gradient and inertia forces, and it depends on the tether current and the mass distribution of the system. In simulations of tether dynamics, it is generally obtained using numerical methods. Obviously, if the tether current is zero (i.e., for the inert tether), ε vanishes and the instability disappears, but this rather trivial situation is of no interest.

It is clear that the tether current is strongly dependent on the device used to collect electrons. Because the instability increases with the tether current, it seems appropriate to focus on bare tethers because they produce the largest tether currents. Indeed, a previous analysis of the generator mode [12] found that adding an electron-collecting device at the end of a bare tether resulted in only a small gain. When a bare tether is used as a deorbiting device, the electrodynamic parameters of the tether must be tuned to obtain a high drag efficiency and a good adaptation to variable ambient conditions. The current-voltage response of the bare tether has been shown [13,14] to exhibit two ideal regimes: one for short tethers and the other for long tethers.

Presented at the 15th AAS/AIAA Space Flight Mechanics Meeting, Copper Mountain, Colorado, 23–27 January 2005; received 11 October 2005; accepted for publication 28 March 2006.

*Escuela Técnica Superior de Ingenieros Aeronáuticos, Plaza Cardenal Cisneros 3; j.pelaez@upm.es, m.sanjurjo@upm.es.

Recently a new concept has been introduced in this matter: the self-balanced electrodynamic tether (SBET) [15,16]. This concept takes advantage of the properties of the tether current profile, especially in the case of bare tethers. In an SBET, the Lorentz torque about the system center of mass becomes zero (or negligible), even for a large tether current. Thus, for an SBET, the parameter ε vanishes when current is flowing in the wire. The balance condition is obtained by appropriately adjusting the system mass distribution, and it results (to a first approximation) in a Lorentz torque that is almost independent of the tether current. This is the key point of the concept: the successful combination of high currents in the tether with very small values of the Lorentz torque.

Recently, the SBET concept has been used in a work for the ESA (see [17]). It is especially interesting in the analysis of the dynamics of satellite orbit descent–ascent using electrodynamic tethers as thrusters, particularly when a high tether current is expected. For example, the concept would be advantageous for keeping large masses (e.g., the International Space Station) in LEO, compensating the aerodynamic drag with a thrusting tether; similarly, in missions to the giant planets, where high orbital velocities and high magnetic fields suggest high tether currents.

The balance condition requires a detailed design of the end masses. It depends on some nominal conditions that must be specified for each particular mission. The electron collection depends on the ionospheric plasma density n_∞. Bare tethers collect electrons in a segment of length L_B (anodic segment), and they exhibit an interesting property: when n_∞ increases (decreases), L_B decreases (increases). This self-regulating property of the bare tethers makes it easy to operate them close to the nominal conditions (i.e., with low values of the Lorentz torque), and hence the instability takes a long time to develop. This makes it unnecessary to use additional devices to control the system attitude dynamic. However, if control is required for safety reasons, the SBET is also readily controllable.

The SBET concept offers an additional advantage. If the tether is flexible, the balance condition will facilitate the analysis of its dynamic response to this type of instability. As a consequence, the influence of the electrodynamic forces on the tether vibrations will be felt more clearly. Note that a zero Lorentz torque obstructs the transfer of energy between the rigid body motion of the tether and its vibrational modes, leading to a more stable system.

However the concept also has some limitations. It is not clear, at present, that the SBET concept would remove the instability from the vibrational motion of the tether, especially when small end masses are involved. Some simulations performed in our group have shown that such behavior is smooth, but this must be studied in further detail. Moreover, in some cases the mass distribution is given beforehand or is totally determined by other mission requirements, and hence the tether system cannot fulfill the balance condition, in general, and the SBET concept as described in this paper would be unusable.

The balance condition has been obtained for two cases [15,16]: 1) for an isolated tether terminated with a spherical collector and 2) for a floating bare tether; that is, a bare tether without a cathodic contactor and for which the current is zero at both ends.

For the floating bare tether, the balance condition does not exhibit sensitivity with the ionospheric plasma density. In other words, the balance condition is very robust for this type of tether. As a consequence, for a balanced tether, the orbit of the center of mass could undergo significant height variations without any substantial change in the Lorentz torque, thereby keeping the tether balanced. However, the balance condition exhibits a small sensitivity to the electric field induced by the Earth's magnetic field E_m. Because E_m changes during the orbit (with the tether position in the orbital frame and with the orbit itself), the tether system only fulfills the balance condition exactly for a particular value of E_m. If this nominal condition is taken as the average value of E_m during the orbit with the tether frozen on the local vertical, tether motion will result in the Lorentz torque oscillating around zero with a maximum excursion bounded by, approximately, 1 deg in the mass angle ϕ. Such a residual torque, which has no significant effects on the tether dynamics, could be readily controlled if needed. In fact, the balanced tethers investigated by simulations in our group have never been destabilized.

The balance condition can be extended without significant difficulties to other types of bare tethers (e.g., nonfloating). Such extension requires a detailed knowledge of the mission to be performed by the tether system. We therefore extend the analysis to obtain the balance condition for electrodynamic tethers working in the generator regime. The goal of this study was to elucidate how the main parameters involved in the analysis influence the balance condition. We selected the deorbiting regime of the electrodynamic tether for two reasons:

1) The mathematics are simpler in this regime than in the thruster regime.

2) There are significant applications for this regime, especially in mitigating space debris.

In addition, a strategy aimed at keeping the tether balanced while taking into account the entire trajectory followed by the system during the deorbiting process is proposed. The dynamic instabilities of electrodynamic tethers can be overcome in other ways, but we believe that balancing the tether is intrinsically interesting and hence worth analyzing.

Dumbbell Model and Governing Equations

We use the dumbbell model to introduce the main features of the SBET concept. In this model, the tether is considered as a rigid rod with two end masses. A detailed deduction of the tether-governing equations using the dumbbell model (for the general elliptic case) can be found elsewhere [18,19].

The significant features of the system dynamics for the circular case have been described previously [15,16]. We will assume a circular inclined orbit, and for the sake of brevity we will use the same nomenclature as described elsewhere [15,16]. In the orbital frame $Gxyz$ (see Fig. 1), the position of the tether and its unit vector $\vec{\boldsymbol{u}}$ are defined by the in-plane angle θ and the out-of-plane angle φ, which will be taken as generalized coordinates.

The tether-governing equations take the form

$$\ddot{\theta} - 2(1+\dot{\theta})\dot{\varphi}\tan\varphi + \tfrac{3}{2}\sin 2\theta = f_\theta \tag{1}$$

$$\ddot{\varphi} + \sin\varphi\cos\varphi[(1+\dot{\theta})^2 + 3\cos^2\theta] = f_\varphi \tag{2}$$

where the electrodynamic forcing terms f_θ and f_φ are given by

$$f_\theta = -\varepsilon(\sin i\tan\varphi[2\sin\nu\cos\theta - \cos\nu\sin\theta] + \cos i) \tag{3}$$

$$f_\varphi = \varepsilon\sin i(2\sin\nu\sin\theta + \cos\nu\cos\theta) \tag{4}$$

Here, the independent variable is the true anomaly ν. The equations must be integrated starting from the following initial conditions:

$$\nu = \nu_0\colon\ \theta = \theta_0, \qquad \varphi = \varphi_0, \qquad \dot{\theta} = \dot{\theta}_0, \qquad \dot{\varphi} = \dot{\varphi}_0 \tag{5}$$

when the tether current is switched on. Equations (1) and (2) involve two free parameters, the inclination i and ε, where the latter parameter gauges the Lorentz torque vs the torque produced by the

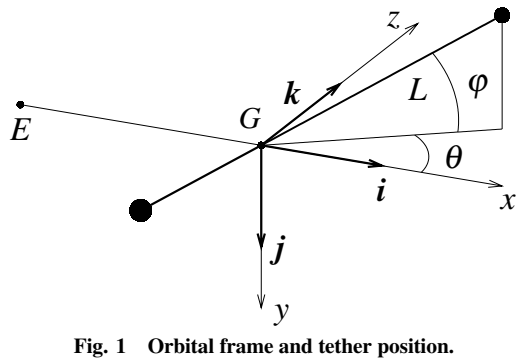

Fig. 1 Orbital frame and tether position.

gravity and inertia forces:

$$\varepsilon = \frac{J_1}{I_s}\frac{\mu_m}{\mu_E} \tag{6}$$

where

μ_E = the gravitational constant of the Earth
μ_m = the strength of the magnetic dipole used to describe the geomagnetic field
I_s = the moment of inertia relative to a line perpendicular to the tether through G
J_1 = an integral expression appearing in the Lorentz torque [see Eq. (7)]

Note that the Lorentz torque about G produced by the tether current profile $I_e(h)$ is

$$\vec{\boldsymbol{M}}_E = \vec{\boldsymbol{u}} \times (\vec{\boldsymbol{u}} \times \vec{\boldsymbol{B}})J_1$$

where

$$J_1 = \int_0^L (h_G - h) I_e(h)\, \mathrm{d}h \tag{7}$$

In Eq. (7), h is the integration variable (see Fig. 2), $h_G = L\cos^2\phi$ is the distance h for the center of mass G, L is the tether length, and $\vec{\boldsymbol{B}}$ is the Earth's magnetic field, which will be considered constant along the tether and equal to its value in G [1,2,19].

Instead of m_1, m_2, and m_t, it is more convenient to use the parameters m, ϕ, and Λ_t. Here, $m = m_1 + m_2 + m_t$ is the total mass of the system, $\Lambda_t = m_t/m$ is a nondimensional tether mass, and ϕ is the mass angle defined by

$$\cos^2\phi = \tfrac{1}{m}\left\{m_1 + \tfrac{1}{2}m_t\right\} \tag{8}$$

$$\sin^2\phi = \tfrac{1}{m}\left\{m_2 + \tfrac{1}{2}m_t\right\} \tag{9}$$

which is a measure of the mass distribution between the two end masses. The mass angle ϕ is in the range of $\mathcal{I} = [\phi_{\min}\text{–}\phi_{\max}]$ where

$$\phi_{\min} = \arcsin\left(\sqrt{\Lambda_t/2}\right), \qquad (m_2 = 0),$$

$$\phi_{\max} = \arccos\left(\sqrt{\Lambda_t/2}\right), \qquad (m_1 = 0)$$

If $\Lambda_t = 0$, then $\mathcal{I} = [0, \pi/2]$. For fixed values of $\Lambda_t = 0$ and m, when ϕ covers the range of $\mathcal{I}$ from $\phi_{\min}$ to $\phi_{\max}$, mass is redistributed from the lower particle to the upper one, and the total mass m does not change. If the two end masses are equal, $\phi = \pi/4$.

Summary of Previous Stability Analysis

If $\varepsilon = 0$, Eqs. (1) and (2) exhibit stable equilibrium positions ($\theta = 0, \pi$, and $\varphi = 0$) with the tether aligned along the local vertical.

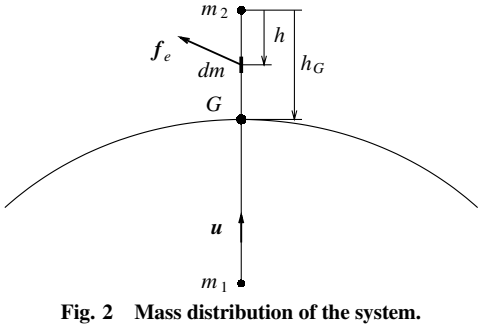

Fig. 2 Mass distribution of the system.

But, if $\varepsilon \neq 0$, instead of equilibrium positions, they exhibit periodic solutions with the orbital period (2π in nondimensional variables). These have been analyzed previously [1,2] using asymptotic techniques in the limit $\varepsilon \to 0$ and also for ε of order unity [6,7]. For each pair of values (ε, i), the analysis yields 1) a special 2π-periodic solution that reduces to the equilibrium position ($\theta = \varphi = 0$) when $\varepsilon = 0$, 2) their monodromy matrix, and 3) the moduli of its eigenvalues, which give the stability properties of the orbit (see [2,7]). The monodromy matrix eigenvalues are two couples of complex conjugate numbers, whose moduli are given (to order ε^3) by

$$|\lambda_{1,2}| = 1 + \tfrac{\pi}{9}\cos i \sin^2 i\varepsilon^3 + O(\varepsilon^4), \qquad \text{if } \varepsilon > 0 \Rightarrow |\lambda_{1,2}| > 1,$$

$$|\lambda_{3,4}| = 1 - \tfrac{\pi}{9}\cos i \sin^2 i\varepsilon^3 + O(\varepsilon^4), \qquad \text{if } \varepsilon < 0 \Rightarrow |\lambda_{3,4}| > 1$$

As a consequence, in the absence of damping or control, the periodic orbit is always unstable. The Lorentz torque about G, which is proportional to ε, causes a periodic excitation of Eqs. (1) and (2). A nonlinear resonance 1:2 is then produced, and the system becomes unstable due to a mechanism that ends by introducing a net flux of energy into the system. Note that any initial deviation Δ from the basic 2π-periodic solution roughly multiplies each orbit by $1 + f_g$; that is, after n orbits, the initial deviation becomes approximately $(1 + f_g)^n\Delta \approx (1 + nf_g)\Delta$, where the growth factor is $f_g \approx ||\lambda| - 1|$. For small values of ε, f_g is given by

$$f_g = ||\lambda| - 1| = \tfrac{\pi}{9}|\cos i|\sin^2 i\varepsilon^3 + O(\varepsilon^4) \tag{10}$$

and it is also small. The growth factor roughly reflects the strength of the instability. It exhibits a cubic dependence on ε, and hence one design goal of a given electrodynamic tether is to make ε as small as possible, within the limits imposed by the system in which the tether will operate.

Assuming that ε is constant and independent of i, f_g is proportional to $\cos i \sin^2 i$, the instability mechanism grows with i and reaches a maximum at $i = \arctan\sqrt{2} \simeq 54.74\,\text{deg}$. For actual tethers, however, ε depends on the inclination i and this result is not realistic.

Tether Current Profile

The description of the electrodynamic performance of bare tethers presented here closely follows a previous analysis [13,14]. If the diameter of the tether is smaller than the Debye length, the electron collection takes place in the orbital-motion limited (OML) regime [20]. There are two tether segments: 1) one of length L_B that collects electrons and 2) one of length $L - L_B$ that collects ions. In the deorbiting regime of the tether, the governing equations for the electron collection are:

$$h < L_B\text{:}\ \frac{\mathrm{d}I_e}{\mathrm{d}h} = en_\infty \frac{p}{\pi}\sqrt{\frac{2e}{m_e}\Phi} \tag{11}$$

$$\frac{\mathrm{d}\Phi}{\mathrm{d}h} = \frac{I_e}{\sigma A_t} - E_m \tag{12}$$

$$h > L_B\text{:}\ \frac{\mathrm{d}I_e}{\mathrm{d}h} = -en_\infty \frac{p}{\pi}\mu\sqrt{\frac{2e}{m_e}|\Phi|} \tag{13}$$

$$\frac{\mathrm{d}\Phi}{\mathrm{d}h} = \frac{I_e}{\sigma A_t} - E_m \tag{14}$$

Here the tether current profile $I_e(h)$ and the potential drop between tether and plasma $\Phi = V_t - V_p$ are the dependent variables. The other parameters are the electrical conductivity σ, the electron charge e, the perimeter of the tether cross section p, the cross section of the conductive portion of the tether A_t, the electron mass m_e, the ion mass m_i, $\mu = \sqrt{m_e/m_i}$, the induced electric field E_m, and the ionospheric plasma density n_∞. Note that the external fields provide

the free parameters E_m and n_∞, which are the most important determinants of the electron collection process.

Equations (11–14) should be integrated together with the following boundary and initial conditions (15–17):

$$\text{at} \quad h = 0\text{: } I_e = 0 \tag{15}$$

$$\text{at} \quad h = L\text{: } I_e = I_C \tag{16}$$

$$\text{at} \quad h = L_B\text{: } \Phi = 0, \qquad I_e = I_B \tag{17}$$

In these equations, L_B, the maximum tether current I_B and I_C are unknowns, and are obtained as a part of the solution. Assuming that I_C is known, the boundary value problem [Eqs. (11–14) and boundary conditions (15–17)] turns out to be mathematically closed, and it provides the profiles $I_e(h)$ and $\Phi(h)$ and the parameters L_B and I_B. However, I_C is unknown and therefore we need one additional relation in order to determine this value: the tether circuit equation, as considered next.

The Tether Circuit Equation

The cathodic contactor at the lower end of the tether adjusts the tether potential to the plasma potential. The potential drop in the cathodic contactor V_{cc} includes two contributions: 1) that due to the contact impedance between the plasma contactor and iohosphere and 2) the wave radiation losses. In addition, let Z_T be any interposed load at the cathodic end of the tether. Figure 3 is a sketch of the tether profiles in the ideal case when $V_{cc} = 0$.

The tether circuit equation can be obtained from Fig. 3 by expressing the potential drop between the tether points C and B in two forms:

$$V_{cc} + I_C Z_T + \Delta V_{BC} = E_m(L - L_B) \tag{18}$$

where the potential drop due to ohmic effects along the BC segment of the tether ΔV_{BC} is given by

$$\Delta V_{BC} = \frac{1}{\sigma A_t}\int_{L_B}^{L} I_e(h)\,\mathrm{d}h \tag{19}$$

Equation (18) is the additional relation that we need to mathematically close the boundary value problem described by Eqs. (11–14) and boundary conditions (15–17).

Nondimensional Equations

Let L_* be the characteristic length given by

$$L_* = \frac{(m_e E_m)^{1/3}}{e 2^{7/3}}\left(3\pi\frac{\sigma h_t}{n_\infty}\right)^{2/3}$$

which is typical of bare tethers and where $h_t = 2A_t/p$ is a characteristic transversal length (for a cylindrical tether is equal to the radius of the wire). The following nondimensional variables are introduced to allow the equations to be integrated:

$$\xi = h/L_* \in [0, \ell_t], \qquad \ell_t = L/L_* \qquad I_e = I_{sc} i_e(\xi)$$
$$\varphi_e = \Phi/(E_m L_*)$$

where $I_{sc} = \sigma E_m A_t$ is the short-circuit current.

In nondimensional variables, Eqs. (11–14) take the form

$$(\xi \le \xi_B) \qquad \frac{\mathrm{d}i_e}{\mathrm{d}\xi} = \frac{3}{4}\sqrt{\varphi_e} \tag{20}$$

$$(\xi \ge \xi_B) \qquad \frac{\mathrm{d}i_e}{\mathrm{d}\xi} = -\frac{3}{4}\mu\sqrt{|\varphi_e|} \tag{21}$$

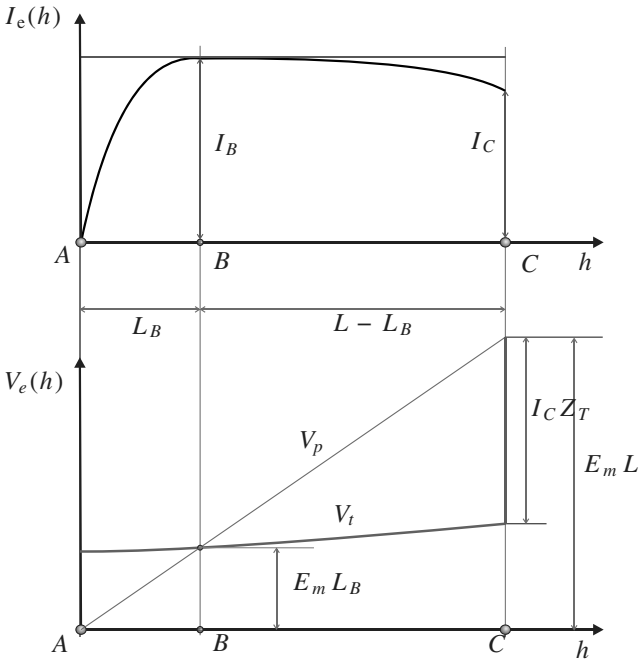

Fig. 3 Tether current and potential profiles.

$$\frac{\mathrm{d}\varphi_e}{\mathrm{d}\xi} = i_e - 1 \tag{22}$$

where $\xi_B = L_B/L_*$. In nondimensional variables, the boundary conditions take the form

$$\xi = 0\text{: } i_e = 0 \tag{23}$$

$$\xi = \xi_B\text{: } \varphi_e = 0, \qquad i_e = i_B \tag{24}$$

$$\xi = \ell_t\text{: } i_e = i_C \tag{25}$$

The potential drop ΔV_{BC} in Eq. (18) can be written as

$$\frac{\Delta V_{BC}}{E_m L_*} = \int_{\xi_B}^{\ell_t} i_e(\xi)\,\mathrm{d}\xi = \int_{\xi_B}^{\ell_t}\left(1 + \frac{\mathrm{d}\varphi_e}{\mathrm{d}\xi}\right)\mathrm{d}\xi = \ell_t - \xi_B + \varphi_C$$

and the complete tether circuit [Eq. (18)] takes the following nondimensional form

$$(\Omega i_C + \tilde{V}_{cc})\ell_t + \varphi_C = 0 \tag{26}$$

where φ_C is the potential bias at the cathodic end, $\tilde{V}_{cc} = V_{cc}/(E_m L)$ is the nondimensional form of V_{cc} and $\Omega = Z_T/R_T$ is the nondimensional form of the interposed load Z_T (here, $R_T = L/(\sigma A_t)$ is the electrical resistance of the tether).

Thus, determining the tether current profile requires the boundary value problem given by Eqs. (20–22), initial and boundary conditions (23–25), and tether circuit equation (26) to be solved. The problem must be tackled numerically to obtain the following parameters: 1) the profiles of $i_e = i_e(\xi; \ell_t, \Omega, \mu, \tilde{V}_{cc})$ and $\varphi_e = \varphi_e(\xi; \ell_t, \Omega, \mu, \tilde{V}_{cc})$, 2) the maximum current $i_B = i_B(\ell_t, \Omega, \mu, \tilde{V}_{cc})$, 3) the current at the cathodic end $i_C = i_C(\ell_t, \Omega, \mu, \tilde{V}_{cc})$, and 4) the length of the tether anodic segment, $\xi_B = \xi_B(\ell_t, \Omega, \mu, \tilde{V}_{cc})$

The integration of the problem (20–26) is straightforward [21].

The value of $\mu = \sqrt{m_e/m_i}$ is small, and depends on the presence of ions of different species. The most abundant ion in the ionosphere is the atomic oxygen O^+ for which $\mu \approx 1/172$. At present, the more promising cathodic contactors are hollow-cathode devices, for which the potential drop V_{cc} takes values in the range of 15–30 V, which is very small compared with the expected value of potential $E_m L$ for a

tether that is several kilometers long. We therefore take $\mu = 1/172$ and $\tilde{V}_{cc} = 0$ in the following analysis.

Balance Condition

Introducing the nondimensional variables, the integral J_1 defined in Eq. (7) becomes

$$\frac{J_1}{\sigma E_m A_t L_*^2} = \int_0^{\ell_t} (\ell_t \cos^2\phi - \xi) i_e(\xi)\, \mathrm{d}\xi \tag{27}$$

and ε can be written as

$$\varepsilon = \varepsilon_0 \cdot \hat{f} \tag{28}$$

where

$$\varepsilon_0 = \frac{E_m}{L} \frac{12\Lambda_t}{(3\sin^2 2\phi - 2\Lambda_t)} \cdot \frac{\mu_m}{\mu_E} \frac{\sigma}{\rho_v} \tag{29}$$

$$\hat{f} = \int_0^{\ell_t} \left(\cos^2\phi - \frac{\xi}{\ell_t} \right) i_e(\xi) \frac{\mathrm{d}\xi}{\ell_t} \tag{30}$$

In this way ε has been split in two factors: ε_0 and $\hat{f}$. Apart from the ratio μ_m:μ_E, ε_0 depends on the tether material (σ/ρ_v, where ρ_v is the material density), the mass distribution (through ϕ and Λ_t), and the ratio E_m/L. It takes values of order unity, except when ϕ is close to the ends of the range of $\mathcal{I} = [\phi_{\min}$–$\phi_{\max}]$. As an example, let us consider a 20-km-long tether comprising a tape with the following dimensions:

$$t = 0.18 \text{ mm (thickness)}, \qquad p \simeq 24 \text{ mm (perimeter)} \tag{31}$$

Figure 4 plots ε_0 vs ϕ for several values of Λ_t, for the following values:

$$\sigma = 3.5 \cdot 10^7 \Omega^{-1} \text{ m}^{-1}, \qquad \rho_v = 2700 \text{ kg/m}^3$$
$$E_m = 165 \text{ V/Km}$$

These values correspond to a tether made of aluminum in a circular orbit inclined 25 deg, at an altitude of 400 km. However, different configurations do not substantially change the values of ε_0, which remains of order unity.

The Lorentz torque and the parameter ε depend on the ionospheric plasma density n_∞. This dependence takes place essentially through the parameter $\hat{f} = \hat{f}[\phi, i_e(\xi)]$ which should be calculated numerically together with the current profile $i_e(\xi)$. Taking into account the nondimensional equations (20–22), the parameter $\hat{f}$ can be rewritten as

$$\hat{f} = \cos^2\phi \frac{U_1(\ell_t, \Omega)}{\ell_t} - \frac{U_2(\ell_t, \Omega)}{\ell_t^2}$$

where $U_1(\ell_t, \Omega)$ and $U_2(\ell_t, \Omega)$ are defined by the following integrals:

$$U_1(\ell_t, \Omega) = \int_0^{\ell_t} i_e(\xi)\, \mathrm{d}\xi, \qquad U_2(\ell_t, \Omega) = \int_0^{\ell_t} \xi i_e(\xi)\, \mathrm{d}\xi \tag{32}$$

Therefore, $\hat{f}(\phi, \ell_t, \Omega)$ must be determined for the different regimes appearing in the problem.

The balance condition takes the simple form $\hat{f} = 0$ and leads to the following mass angle:

$$\cos\phi^* = \sqrt{\frac{U_2(\ell_t, \Omega)}{\ell_t U_1(\ell_t, \Omega)}} \tag{33}$$

assuring that the Lorentz torque vanishes.

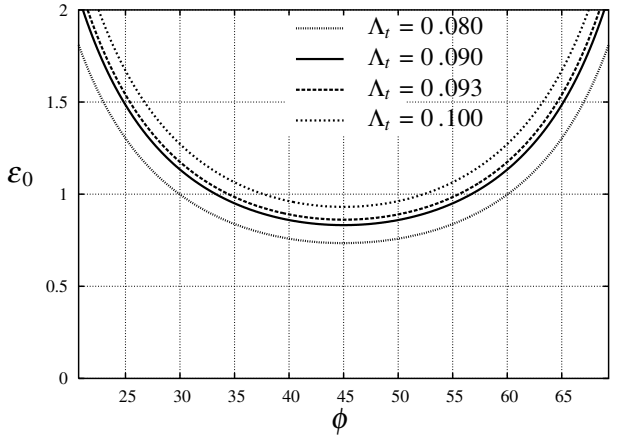

Fig. 4 Parameter ε_0.

Power

For a bare tether working in the generator regime, there are two significant parameters related to the power developed by the electrodynamic forces acting on the system: 1) the power dissipated in the whole system W_d and 2) the power obtained in the interposed load Z_T, W_g.

The first term gives the loss of mechanical energy associated with the deorbiting process, and the second one is the energy that can be used onboard the orbiter to perform some task.

Let $\vec{B}$ be the Earth's magnetic field. The electrodynamic force acting on a tether element and the power dissipated by this force are

$$\vec{f} = I_e(h)\vec{u} \times \vec{B}\, \mathrm{d}h, \qquad W_d^{dh} = \vec{v}_G \cdot (\vec{u} \times \vec{B}) I_e(h)\, \mathrm{d}h$$

where, as an approximation, the velocity of the element is assumed to be equal to the velocity $\vec{v}_G$ of the system center of mass. The overall dissipated power will be

$$W_d = \vec{v}_G \cdot (\vec{u} \times \vec{B}) \int_0^L I_e(h)\, \mathrm{d}h = -E_m \int_0^L I_e(h)\, \mathrm{d}h$$

because the component of the electric field induced by the Earth's magnetic field along the tether direction is given by

$$E_m = \vec{u}_G \cdot (\vec{v} \times \vec{B}) \tag{34}$$

In terms of the nondimensional variables, the preceding expression takes the form:

$$W_d = -E_m L I_{sc} \frac{1}{\ell_t} \int_0^{\ell_t} i_e(\xi)\, \mathrm{d}\xi = -E_m L I_{sc} \frac{U_1(\ell_t, \Omega)}{\ell_t}$$

and $U_1(\ell_t, \Omega)$ can be calculated as follows:

$$U_1(\ell_t, \Omega) = \int_0^{\ell_t} i_e(\xi)\, \mathrm{d}\xi = \ell_t - \varphi_A + \varphi_C$$

where φ_A (φ_C) is the potential bias at the anodic (cathodic) end. In nondimensional terms we have

$$\frac{W_d}{E_m L I_{sc}} = -\left\{ 1 - \frac{\varphi_A - \varphi_C}{\ell_t} \right\} = -\eta_t$$

where

$$\eta_t = 1 - \frac{\varphi_A - \varphi_C}{\ell_t} \tag{35}$$

and this last parameter is a suitable measure of the tether efficiency as a deorbiter.

The power obtained in the interposed load is given by

$$W_g = I_C^2 Z_T = E_m L I_{sc} i_C^2 \Omega$$

which, taking into account the tether-circuit equation (26), can be written as

$$\frac{W_g}{E_m L I_{\rm sc}} = i_C\left(\frac{|\varphi_C|}{\ell_t} - \tilde{V}_{\rm cc}\right) \approx \frac{i_C|\varphi_C|}{\ell_t} \tag{36}$$

Deorbiting in the Ideal Case

For deorbiting applications, the interposed load Z_T must be as small as possible in order to minimize the power generated [Eq. (36)]. The limit in which $Z_T = 0$ is taken as the ideal case, which has been analyzed previously [13,14]. In this section, we summarize the main characteristics of this regime following that analysis closely and assuming $\tilde{V}_{\rm cc} = 0$.

Because μ is small, Eqs. (21–25) for $\xi > \xi_B$ have the solution $\varphi_e(\xi) \approx -(1 - i_B)(\xi - \xi_B)$ and $i_e(\xi) \approx i_B \approx i_C$. Thus, the final value of φ_C is $\varphi_C = -(1 - i_B)(\ell_t - \xi_B)$. However, when $\Omega = 0$, the tether-circuit equation (26) provides $\varphi_C = 0$, and this condition holds under only two conditions: either $i_B = 1$ or $\ell_t = \xi_B$. This gives rise to two regimes for fulfilling $\varphi_C = 0$:

1) If $\ell_t < 4$ and $\ell_t = \xi_B$, this is the short tether regime.

2) If $\ell_t \geq 4$ and $i_B = 1$, this is the long tether regime.

Short Tether Regime

In the short tether regime, the segment BC disappears; that is, the entire tether is inside the anodic segment AB. Therefore, in this regime the relation $\ell_t = \xi_B$ is always satisfied.

Figure 5 shows, on the left side, the current and the potential profiles of the tether for different maximum tether currents $i_B = 0.25$, 0.5, 0.85, and 1.0.

Integrals U_1 and U_2, defined in Eq. (32), must be extended to the range of 0–ξ_B, and take the following values:

$$U_1(\ell_t, 0) = \ell_t - \varphi_A = \xi_B - [i_B(2 - i_B)]^{\frac{2}{3}}$$

$$U_2(\ell_t, 0) = \frac{1}{2}\xi_B^2 - \frac{4}{3}(1 - i_B)^{\frac{5}{3}} \int_0^{v_0} \sinh^{\frac{5}{3}} u \, {\rm d}u$$

where v_0 is defined by the relation $\cosh v_0 = (1 - i_B)^{-1}$. Because $\xi_B = \xi_B(i_B)$, both parameters only depend on i_B. The power dissipated by the system in this regime is

$$\frac{W_d}{E_m L I_{\rm sc}} = -\left\{1 - \frac{[i_B(2 - i_B)]^{\frac{2}{3}}}{\xi_B}\right\}$$

and hence is also a function of i_B.

The upper extreme of this segment appears for $\ell_t = \xi_B = 4$ and $i_B = 1$, where the transition to the long tether regime takes place.

Long Tether Regime

In the long tether regime, $i_B = 1$ and $\xi_B = 4$, and the solution for the cathodic segment $\xi > \xi_B$ is trivial: $\varphi_e(\xi) \equiv 0$ and $i_e(\xi) \equiv 1$.

Figure 5 shows, on the right side, the current and the potential profiles of the tether for a tether length of $\ell_t = 10$. For different values of $\ell_t > 4$, the only difference is in the extension of the cathodic segment.

Integrals U_1 and U_2 must be extended now to the entire tether $[0, \ell_t]$ and take the following values:

$$U_1(\ell_t, 0) = \ell_t - 1, \qquad U_2(\ell_t, 0) = \tfrac{36}{5} + \tfrac{1}{2}(\ell_t^2 - 16) = \tfrac{1}{2}\left(\ell_t^2 - \tfrac{8}{5}\right)$$

The power dissipated by the system in this regime is

$$\frac{W_d}{E_m L I_{\rm sc}} = -\left\{1 - \frac{1}{\ell_t}\right\}$$

and is only a function of ℓ_t.

Deorbiting Tether Efficiency

Parameter η_t, defined in Eq. (35), is a suitable measure of the tether efficiency as deorbiter. The expressions obtained for the short and long regimes permit plotting this parameter as a function of the tether length ℓ_t, as in Fig. 6. Note that

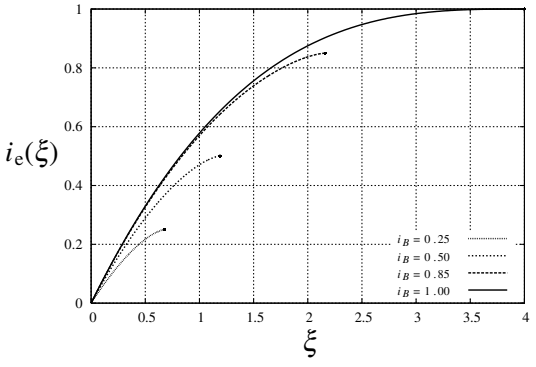

Short tether regime: current $i_e(\xi)$

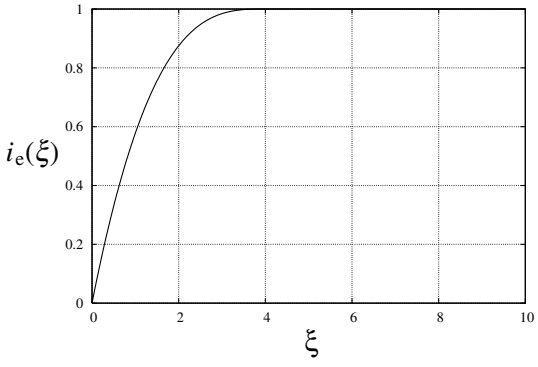

Long tether regime: current $i_e(\xi)$

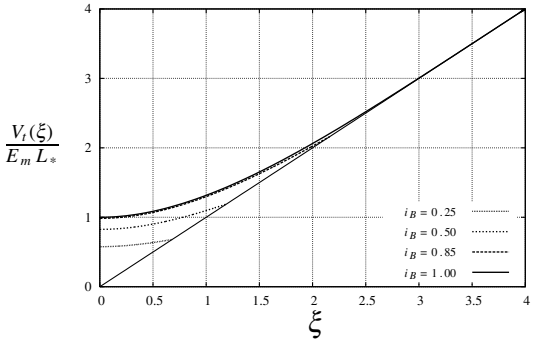

Short tether regime: potential $V_t(\xi)$

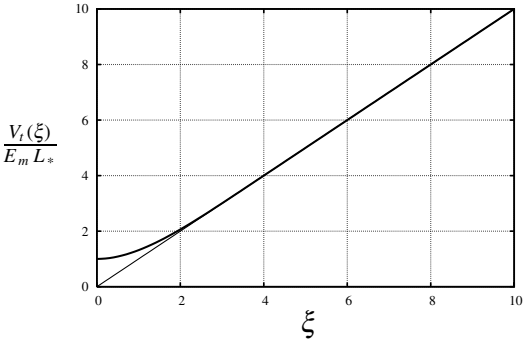

Long tether regime: potential $V_t(\xi)$

Fig. 5 Current and potential profiles of the tether. Short tether regime in the left, long tether regime in the right.

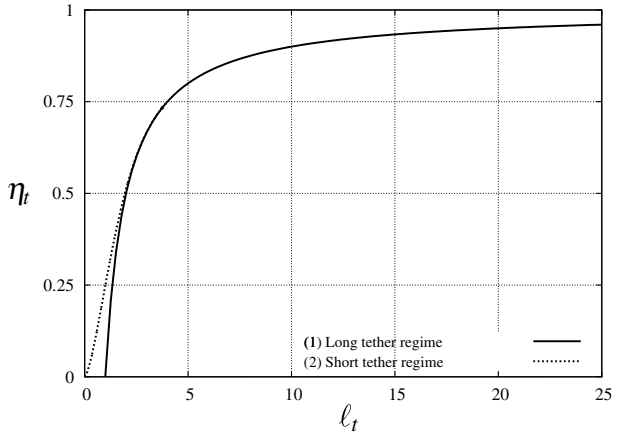

Fig. 6 Dissipated power vs ℓ_t.

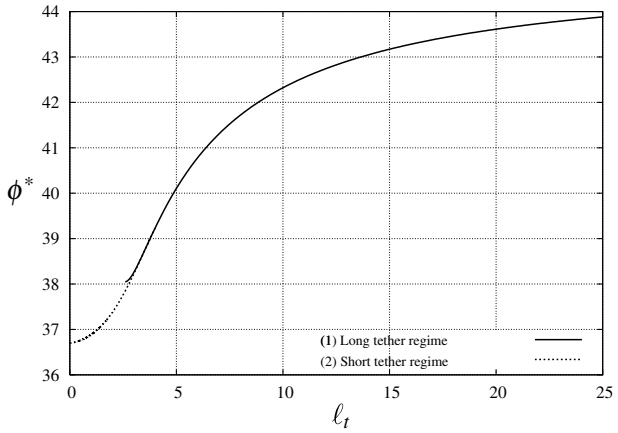

Fig. 7 Mass angle critical value ϕ^*, deg vs ℓ_t.

1) The tether efficiency in the long tether regime extends for values of ℓ_t down to $\approx$2.

2) The efficiency clearly increases with the tether length ℓ_t.

Balance Condition

The critical value of the mass angle ϕ as given in balance condition (33) is only a function (in this ideal case) of the tether length, ℓ_t. Figure 7 plots this function, taking into account the expressions obtained previously for the functions U_1 and U_2 defined in Eq. (32).

Figure 6 shows that the performances of the tether increase with the nondimensional tether length. However, ℓ_t is proportional to $n_\infty^{\frac{2}{3}}$ when the other parameters take constant values, and typically the ionospheric plasma density n_∞ varies by one order of magnitude during the orbit. Thus, the ratio of the maximum and minimum values of ℓ_t is about $10^{2/3} \approx 5$ during the orbit. To ensure its effectiveness, the tether must be designed to operate in the approximate range of $\ell_t \in [3\text{–}15]$, for which the values of η_t would be in the range of 0.7–0.95. Figure 7 shows that the critical mass angle for which the tether remains balanced takes values in the approximate range of 38.2–43.2 deg.

If we choose to balance the tether in the middle of the range (i.e., $\ell_t \approx 6$ and $\phi \approx 40.7$ deg), the tether will be unbalanced during almost the entire orbit. However, the magnitude of this unbalanced situation can be described with the help of parameter $\hat{f}$ as defined in Eq. (30), taking $\cos\phi = \cos\phi^* \approx 0.758$. Figure 8 shows the variation of $\hat{f}$ with ℓ_t. Note that $\hat{f} \in [-0.03\text{–}0.04]$ for the case analyzed here, and considering $\varepsilon_0 \approx 1$, the value of ε oscillates in the same range $[-0.03\text{–}0.04]$. The growth factor f_g given by Eq. (10) is $f_g \approx 8 \cdot 10^{-6}$ for $i = 45$ deg. The analysis associated with grow factor f_g cannot be directly applied because ε is not constant in a real

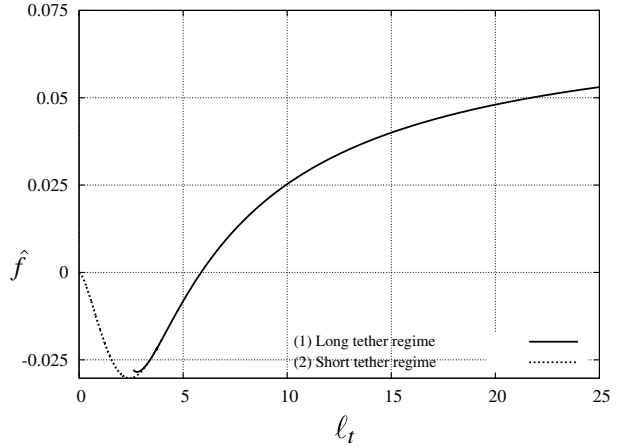

Fig. 8 Values of $\hat{f}$ vs ℓ_t.

tether. However, assuming that ε is constant and in the worst case $\hat{f} = 0.04$, any initial deviation from the periodic solution takes a long time to double ($\approx$10 years in LEO).

In this way, the Lorentz torque remains close to zero during the mission, and hence the effects of the dynamic instability have been minimized. Simultaneously, the deorbiting effectiveness of the tether will remain high, although it will obviously be slightly lower than that shown in Fig. 6 due to the libration of the tether excited by the Lorentz torque. However, the tether could be balanced more accurately if we sacrifice some efficiency, as shown in the next section. It should be noted that the strategy for choosing the critical mass angle ϕ^* can be optimized in several ways, such as by adjusting its value to the averaged expected values of ℓ_t during the orbit.

Deorbiting in the General Case

Some authors distinguish between the deorbiting mode, where $\Omega = 0$ or very small, and the generator mode, where $\Omega \approx \mathcal{O}(1)$. In the first case, the tether is tuned to maximize the orbital decay, and in the second one, it maximizes the power obtained in the interposed load. In this section, we assume Ω is not zero, but still small enough to permit the tether to work in the deorbiting regime. As before, we take $\mu = 1/172$ and $\tilde{V}_{cc} = 0$ in the following analysis.

The problem defined by Eqs. (20–26) must be solved numerically to obtain the profiles of current and potential along the tether

$$i_e = i_e(\xi; \ell_t, \Omega), \qquad \varphi_e = \varphi_e(\xi; \ell_t, \Omega)$$

Moreover, and as a part of the solution, the analysis provides the additional relationships

$$i_B = i_B(\ell_t, \Omega), \qquad i_C = i_C(\ell_t, \Omega) \tag{37}$$

$$\xi_B = \xi_B(\ell_t, \Omega), \qquad \eta_t = \eta_t(\ell_t, \Omega) \tag{38}$$

Figure 9 shows the profiles of the tether current $i_e(\xi)$ and the tether potential $V_t(\xi) = (E_m L_*)(\varphi_e(\xi) + \xi)$ along the tether for $\ell_t = 6$ (selected arbitrarily) and for three values of Ω ($\Omega = 0.0$, 0.05, and 0.1). As expected, because the ion collection has very small effects in the neighborhood of the deorbiting ideal case, $i_B - i_C \ll 1$. Moreover, the tether current profile shows that small variations in Ω result in a clear shortening of the anodic segment (from 4 to 2.5 when Ω changes from 0 to 0.05).

The plot of the potential profile helps explain why the length of the anodic segment is strongly affected by small variations of the interposed load Ω. It should be noted that, for the ideal case $\Omega = 0$, the tether potential profile is tangent to the plasma potential line at $\xi = \xi_B$ ($\xi_B = 4$ in Fig. 9) and coincides with the plasma potential line for $\xi_B \le \xi \le \ell_t$. When $\Omega \neq 0$, the tether potential crosses the plasma potential line at $\xi = \xi_B$ and this point moves down drastically. However, the deorbiting efficiency of the tether as defined in Eq. (35) is not greatly affected by this behavior, as shown next.

Figure 10 plots the additional relationships [Eqs. (37) and (38)], taking ℓ_t as the independent variable and Ω as the parameter. In addition to the ideal case ($\Omega = 0$), the figure considers the following values of Ω: $\Omega = 0.01, 0.02, \ldots, 0.1$ and $\Omega = 0.2$.

Figure 10 demonstrates how the introduction of a nonvanishing value for Ω changes the solution from the ideal case described in the previous section. However, this change is small for the small values of Ω considered here, as expected. The most affected parameter is length ξ_B of the anodic segment, which, as stated previously, changes dramatically even for very small values of Ω. It should be noted that the deorbiting efficiency of the tether η_t clearly decreases with Ω, but still remains close to the ideal case.

The balance condition (33) provides the critical value $\phi^* = \phi^*(\ell_t, \Omega)$. Figure 11 shows this function, taking ℓ_t as the independent variable and Ω as the parameter. It is clear that the mass angle that balances the tether increases with Ω, but for small values of Ω the changes are small.

An important point evident in Fig. 11 is that the tether cannot be balanced by keeping Ω constant. The change in the ionospheric plasma density n_∞ during the orbit changes the nondimensional tether length ℓ_t and, consequently, the critical value ϕ^* will change with ℓ_t. The same problem appeared in the ideal deorbiting case described previously. However, we can improve the results obtained there by using the following procedure:

1) We select a critical value for the mass angle ϕ_0^*, corresponding to a typical value of ℓ_t (e.g., the average value of ℓ_t during the orbit of the center of mass, or the upper value expected during the orbit, would be appropriate).

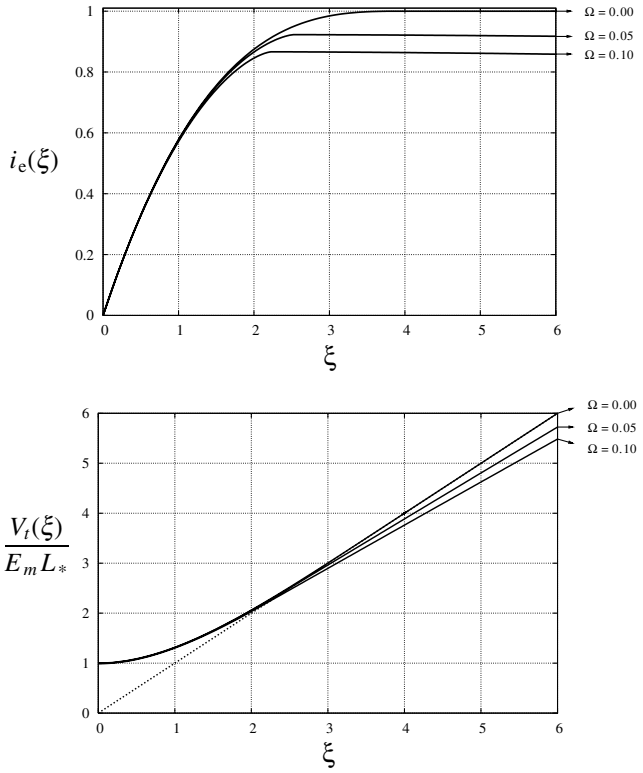

Fig. 9 Profiles of current and potential for $\ell_t = 6$.

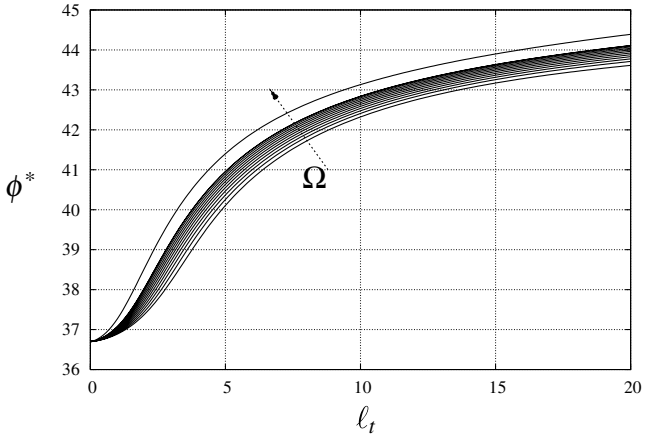

Fig. 11 Balance condition for different values of Ω.

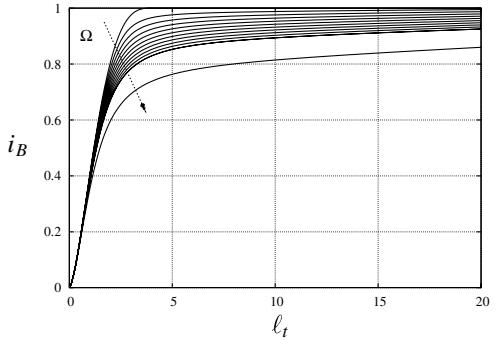

Maximum current i_B

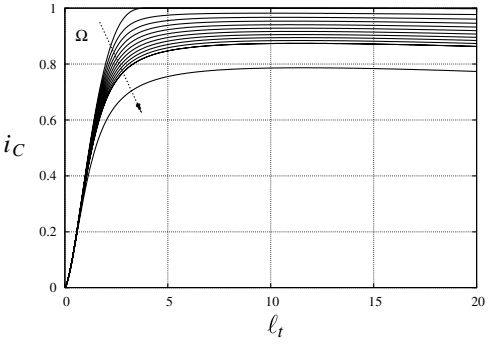

Cathodic current i_C

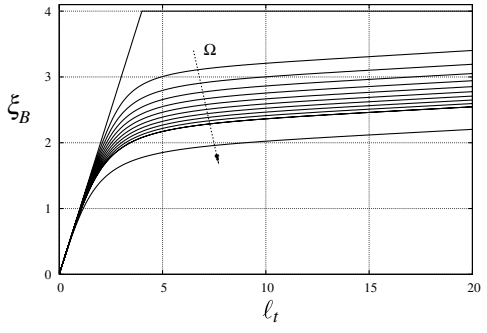

Anodic segment ξ_B

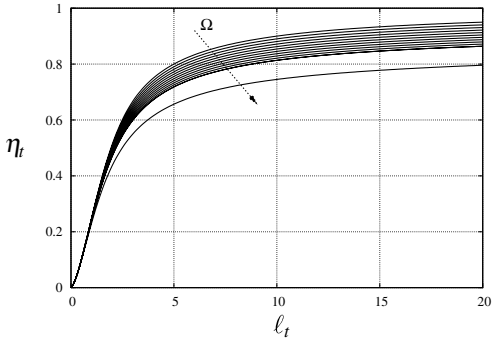

Deorbiting efficiency η_t

Fig. 10 Tether parameters vs ℓ_t for different values of $\Omega = 0, 0.01, 0.02, \ldots, 0.1, 0.2$.

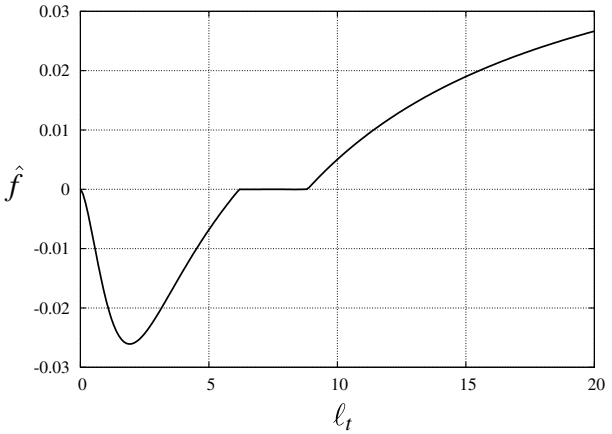

Fig. 12 Balanced tether: $\hat{f}$ vs ℓ_t.

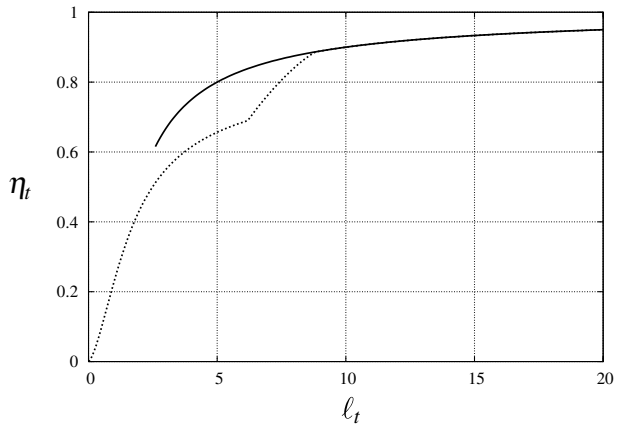

Fig. 13 Balanced tether: η_t vs ℓ_t.

2) Balance condition (33) then provides the relation

$$\cos\phi_0^* - \sqrt{\frac{U_2(\ell_t,\Omega)}{\ell_t U_1(\ell_t,\Omega)}} = 0$$

that gives, for each value of ℓ_t, the value of Ω that keeps the tether balanced:

$$\Omega^* = \Omega^*\left(\phi_0^*, \ell_t\right) \tag{39}$$

3) The preceding relationship can be extended to any range $[a, b]$ of values of ℓ_t if the value of ϕ_0^* is selected appropriately.

We now develop a small example to illustrate the preceding ideas. We assume that $\phi_0^* = 42$ deg and choose to keep the tether balanced in the segment $\ell_t \in [a, b] = [6.18, 8.83]$. The function $\Omega^* = \Omega^*(\phi_0^*, \ell_t)$ defined in Eq. (39) then takes the following form:

$$\begin{aligned} \ell_t < 6.18 &\Rightarrow \Omega^* = 0.2 \\ 6.18 < \ell_t < 8.83 &\Rightarrow \Omega^* = 0.00122\ell_t^4 - 0.03845\ell_t^3 \\ &\quad + 0.47\ell_t^2 - 2.69168\ell_t + 6.18134 \\ \ell_t > 8.83 &\Rightarrow \Omega^* = 0.0 \end{aligned} \tag{40}$$

The expression on the right-hand side of Eq. (40) was fitted to the numerical results using the least-squares method.

Thus, the tether will be exactly balanced in the segment $\ell_t \in [a, b] = [6.18, 8.83]$, but will be unbalanced outside this segment. To assess this unbalanced situation, in Fig. 12 we plot $\hat{f}$ vs ℓ_t using the law in Eq. (40)

$$\hat{f} = \cos^2\phi_0^* \frac{U_1(\ell_t,\Omega^*)}{\ell_t} - \frac{U_2(\ell_t,\Omega^*)}{\ell_t^2}$$

Comparison with the situation described in the ideal case (Fig. 8) reveals two clear advantages:

1) When ℓ_t is in the range of 3–15, the extreme values of $\hat{f}$ are substantially decreased from those in the ideal case (i.e., -0.03 and 0.04) to approximately -0.02 and 0.02, respectively.

2) Along the segment ($a = 6.18$ and $b = 8.83$) the tether is exactly balanced and the Lorentz torque is exactly zero.

However, stabilizing the attitude motion of the system reduces the efficiency of the deorbiting tether. For our example, the drag efficiency of the tether can be calculated as a function of the nondimensional tether length ℓ_t. Figure 13 shows the efficiency of the deorbiting tether η_t as a function of ℓ_t for the law in Eq. (40). The upper line corresponds to the ideal case shown in Fig. 6, and the lower line corresponds to our example. The two lines coincide for $\ell_t > b = 8.83$, but the efficiency is lower for $\ell_t < b$.

It should be noted that the values ϕ_0^* and $[a, b]$ must be tuned for each particular mission, due to variations in the required level of dynamic stability of the tether. The selection of appropriate values will yield a tether that is always balanced during its descent. This continuous balance could represent a very interesting solution for other types of self-balanced tethers that we will present in subsequent papers.

We should emphasize that it is simple to implement the control procedure proposed here. Two main parameters are involved: 1) the ionospheric plasma density n_∞ and 2) the induced electric field E_m; the former can be measured with a cylindrical langmuir probe and the latter can be estimated from the dynamic state of the center of mass G, knowledge of the Earth's magnetic field [the international geomagnetic reference field (IGRF) model is sufficient], and a crude approximation for the tether librations. These parameters can be used to calculate ℓ_t, from which the critical value of the interposed load Ω^* can be obtained. The addition of a potentiometer to the tether circuit allows the value of the interposed load to be readily controlled; this procedure can be improved by measuring the tether current at the cathodic end using a normal ammeter.

All of the results described in this paper were obtained using numerical calculations with Runge–Kutta–Fehlberg 7(8) routines. In some cases, we performed two different calculations (different teams) to assure the accuracy of the numerical results. However, it should be noted that the proposed control scheme is based on several models; in particular, on the OML-regime model used to describe the electron collection of the tether. If these models are valid, the control scheme is also valid and accurate. If the OML (or any other) model is replaced by a more exact one, our control scheme could be adapted to the new model without significant problems.

Deorbiting a Satellite

In this section we present the solution to a deorbiting problem, in which a 1063 kg satellite in a circular orbit with an altitude of about 1000 km and an inclination of 35 deg is deorbited by using the tether described in Table 1 (the natural lifetime of such a satellite is measured in centuries). We compare the performances

Table 1 Characteristic of an example tether

	Self-balanced	Not balanced
Diameter	1.5 mm	1.5 mm
Length	5 km	5 kg
Mass m_1	647.8 kg	1000 kg
Mass m_2	392.2 kg	40 kg
Initial height	1000 km	1000 km
Material	Aluminum	Aluminum
V_{cc}	10 V	10 V
Interposed load	0 Ω	0 Ω
Orbit	Circular	Circular
Date	15 June_2000	15 June 2000

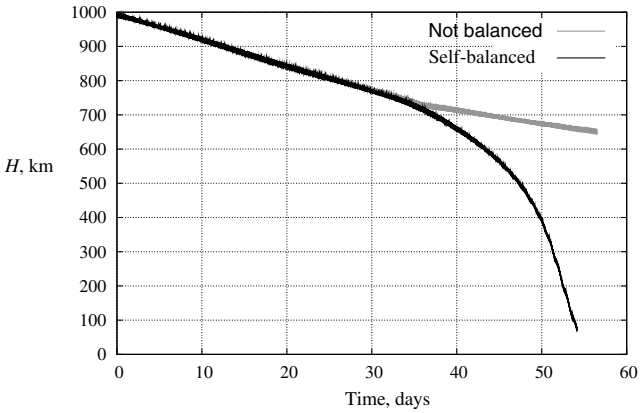

Fig. 14 Perigee height H vs time.

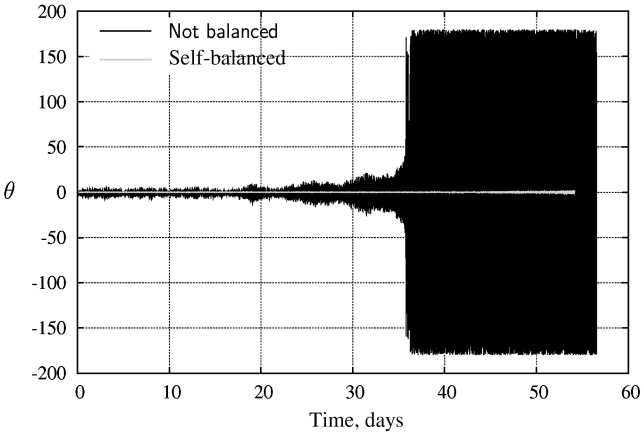

Fig. 15 In-plane libration angle.

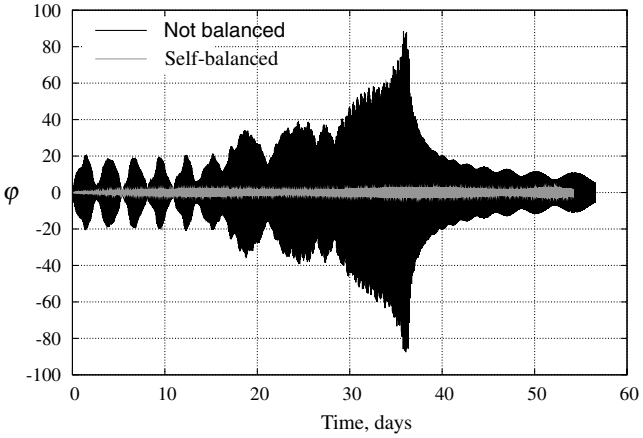

Fig. 16 Out-of-plane libration angle.

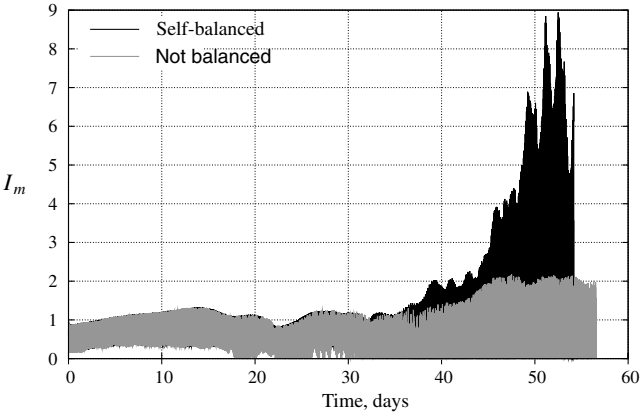

Fig. 17 Averaged tether current.

of self-balanced and not-balanced options for deorbiting this satellite.

We use the dumbbell model to simulate the dynamics, the Earth's magnetic field as given by the IGRF 2000 model, and the ionospheric properties in the IRI 2000 model. The effect of the J_2 harmonic of the Earth's gravity is included, because the regression of the ascending node in the inertial frame affects the ionospheric plasma density during the orbit. However, the aerodynamic drag is excluded to avoid noise in the comparison.

It should be noted that the simulations were performed under the following conditions designed to maximize the dynamic instabilities: the natural damping and the variations of the electrical resistance of a real tether (due to the temperature variations) were ignored, because these help to produce smoother dynamics; and the simulation was performed in an epoch of high solar activity, which assures the highest values of ionospheric plasma density and, consequently, the maximum collected tether current.

Figure 14 shows the time history of the perigee height for both tethers. For the SBET tether the simulation shows very smooth dynamics leading to the deorbiting of the satellite in $\simeq$ eight weeks. In contrast, the nonbalanced tether experiences complex and violent dynamics after $\simeq$ five weeks, a transition from libration to rotation taking place. In the figure, this transition appears as an inflection in the curve of the perigee height.

The transition is very clear in Fig. 15, which plots the time history of the in-plane libration angle for the two types of tethers. After three weeks, the tethered system reaches layers of the ionosphere with increasing plasma density. For the nonbalanced tether, an instability in the attitude dynamics begins to develop, with the transition from libration to rotation taking place approximately two weeks later. In a real tether, this transition would be preceded by violent dynamics that must be avoided. In contrast, the angle θ takes values lower than 1 deg for the self-balanced tether, during the entire descent.

Figure 16 shows the time history of the out-of-plane libration angle for the two types of tethers. Notice that, for the nonbalanced tether, the angle φ reaches almost 90 deg close to the transition time. In contrast, the out-of-plane angle remains in the range of -3–3 deg for the self-balanced tether during the entire descent. For the SBET tether, the dynamics is quite smooth even when the system is traversing the F layer of the ionosphere where the plasma density reaches its maximum values.

Figure 17 shows the average current collected by the tether during the descent in the two cases considered. Note that for the SBET tether, the current reaches peak values of 8–9 A. This figure helps to explain the key point of the SBET concept: the combination of a high tether current with very smooth dynamics.

It should be noted that the simulations performed did not include the lateral dynamics or the vibrational motion of the tether; these should be clarified in the future. However, the dynamic simulations performed in our group with a bead model for similar cases (which included the tether lateral dynamics) have predicted very smooth dynamics also for this motion.

Conclusion

This paper describes how to balance an electrodynamic bare tether operated in a circular inclined orbit in the generator regime. For this type of tether, the balance condition depends on the following factors: 1) the geometric and material characteristics of the tether, 2) the external fields and orbital characteristics, 3) the system mass distribution, and 4) the interposed load.

When the tether is tuned to exhibit good performances as a deorbiter, the interposed load is zero and the tether deorbiting efficiency can be maximized according to the mission requirements. In this deorbiting regime, balancing the tether implies choosing a mass distribution so as to minimize the Lorentz torque. However, the

large variation of the ionospheric plasma density during the orbit prevents the Lorentz torque from always being zero. If desired, the mass distribution can be tuned to obtain a Lorentz torque whose averaged value during the orbit is zero. With this design, the system improves its dynamic stability to yield an excellent solution for some mission requirements in terms of a controlled attitude motion.

The results of the simulations described in this paper demonstrate that the SBET combines a high tether current with very smooth dynamics. However, the possibilities that have not been considered here open a wide range of solutions to be explored in the future. We offer a more sophisticated solution for missions with strong requirements on the dynamic stability of the attitude. Using a small interposed load and sacrificing some of the efficiency of the deorbiting tether makes it possible to introduce a control system that exactly cancels the Lorentz torque for a wide range of ionospheric plasma densities. Some tradeoff between the dynamic stability and the deorbiting efficiency is required for each mission, in order to optimize the procedure.

Finally, we should emphasize that it is simple to implement the control procedure proposed here. The addition of a potentiometer to the tether circuit would make it easy to control the interposed load. An open-loop control system could be implemented by 1) measuring the ionospheric plasma density (with a cylindrical langmuir probe) and 2) estimating the induced electric field from the dynamic state of the system and the IGRF model.

Acknowledgement

This work was performed within the framework of the research project entitled "Dynamics of Satellite Orbit Descent/Ascent Using Electrodynamic Tethers" (ESP2004-04376), supported by the Dirección General de Investigación (DGI) of the Spanish Ministry of Science and Technology.

References

[1] Peláez, J., Lorenzini, E. C., López-Rebollal, O., and Ruiz, M., "A New Kind of Dynamic Instability in Electrodynamic Tethers," *Spaceflight Mechanics 2000*, Advances in the Astronautical Sciences, Vol. 105, Univelt, San Diego, CA, for the American Astronautical Society, Springfield, VA, 2000, pp. 1367–1386.

[2] Peláez, J., Lorenzini, E. C., López-Rebollal, O., and Ruiz, M., "A New Kind of Dynamic Instability in Electrodynamic Tethers," *Journal of the Astronautical Sciences*, Vol. 48, No. 4, Oct.–Dec. 2000, pp. 449–476.

[3] Peláez, J., Ruiz, M., López-Rebollal, O., Lorenzini, E. C., and Cosmo, M. L., "A Two Bar Model for the Dynamics and Stability of Electrodynamic Tethers," *Spaceflight Mechanics 2000*, Advances in the Astronautical Sciences, Vol. 105, Univelt, San Diego, CA, for the American Astronautical Society, Springfield, VA, 2000, pp. 1327–1336.

[4] Peláez, J., Ruiz, M., López-Rebollal, O., Lorenzini, E. C., and Cosmo, M. L., "Two Bar Model for Two Bar Model for the Dynamics and Stability of Electrodynamic Tethers," *Journal of Guidance, Control, and Dynamics*, Vol. 25, No. 6, Nov.–Dec. 2002, pp. 1125–1135.

[5] Peláez, J., López-Rebollal, O., Ruiz, M., and Lorenzini, E. C., "Damping in Rigid Electrodynamic Tethers on Inclined Orbits," *Spaceflight Mechanics 2001*, Advances in the Astronautical Sciences, Vol. 108, Univelt, San Diego, CA, for the American Astronautical Society, Springfield, VA, 2001, pp. 1203–1624.

[6] Peláez, J., and Lara, M., "Periodic Solutions in Rigid Electrodynamic Tethers on Inclined Orbits," *Spaceflight Mechanics 2001*, Advances in the Astronautical Sciences, Vol. 108, Univelt, San Diego, CA, for the American Astronautical Society, Springfield, VA, 2001, pp. 1189–1208.

[7] Peláez, J., and Lara, M., "Periodic Solutions in Electrodynamic Tethers on Inclined Orbits," *Journal of Guidance, Control, and Dynamics*, Vol. 26, No. 9, May–June 2003, pp. 395–406.

[8] Dobrowolny, M., "Lateral Oscillations of an Electrodynamic Tether," *Journal of the Astronautical Sciences*, Vol. 50, No. 2, 2002, pp. 125–147.

[9] Somenzi, L., Iess, L., and Peláez, J., "Linear Stability Analysis of Flexible Electrodynamic Tethers," American Astronautical Society Paper AAS03-539, 2003.

[10] Lorenzini, E. C., Estes, R. D., Cosmo, M. L., and Peláez, J., "Dynamic, Electrical, and Thermal Coupling in a New Class of Electrodynamic Tethered Satellites," Advances in the Astronautical Sciences, Vol. 102, Univelt, San Diego, CA, for the American Astronautical Society, Springfield, VA, 1999, pp. 1333–1344.

[11] Corsi, J., and Iess, L., "Stability and Control of Electrodynamic Tethers for De-Orbiting Applications," *Acta Astronautica*, Vol. 48, No. 5–12, 2001, pp. 491–501.

[12] Samanta Roy, R. I., Hastings, D. E., and Ahedo, E., "Systems Analysis of Electrodynamic Tethers," *Journal of Spacecraft and Rockets*, Vol. 29, No. 3, 1992, pp. 415–424.

[13] Ahedo, E., and Sanmartín, J. R., "Analysis of Electrodynamic Tethers as Deorbiting Systems," AIAA Paper 2000-3763, 2000.

[14] Ahedo, E., and Sanmartín, J. R., "Analysis of Bare-Tether Systems for Deorbiting Low-Earth-Orbit Satellites," *Journal of Spacecraft and Rockets*, Vol. 39, No. 2, 2002, pp. 198–205.

[15] Peláez, J., "Self Balanced Electrodynamic Tethers," AIAA Paper 2004-5309, 2004.

[16] Peláez, J., Sanjurjo, M., and Fontdecaba, J., "Satellite Deorbiting Using a Self Balanced Electrodynamic Tether," International Astronautical Congress Paper IAC-04-A.5.08, 2004.

[17] Sanmartín, J. R., Charro, M., Elaskar, S., Peláez, J., Tinao, I., and Hilgers, A., "Floating Bare-Tether as Upper Atmosphere Probe," ESA/European Space Research and Technology Centre Contract No. 17384/03/NL/LvH/bj, 2004.

[18] Peláez, J., and Andrés, Y. N., "Dynamic Stability of Electrodynamic Tethers in Inclined Elliptical Orbits," *Astrodynamics 2003*, Advances in the Astronautical Sciences, Vol. 116, Univelt, San Diego, CA, for the American Astronautical Society, Springfield, VA, 2004, pp. 595–614.

[19] Peláez, J., and Andrés, Y. N., "Dynamic Stability of Electrodynamic Tethers in Inclined Elliptical Orbits," *Journal of Guidance, Control, and Dynamics*, Vol. 28, No. 4, 2005, pp. 611–622.

[20] Sanmartín, J. R., and Estes, R. D., "The Orbital-Motion-Limited Regime of Cylindrical Langmuir Probes," *Physics of Plasmas*, Vol. 6, No. 1, 1999, pp. 395–405.

[21] Sanmartín, J. R., Martínez-Sánchez, M., and Ahedo, E., "Bare Wire Anodes for Electrodynamic Tethers," *Journal of Propulsion and Power*, Vol. 9, No. 3, 1993, pp. 353–360.

N. Gatsonis
Associate Editor